Supporting Information

Rabbani et al. 10.1073/pnas.1800729115

More Details About the Theoretical Analysis

Theoretical analysis is performed on a 2D porous medium with the length and width in x and y direction denoted as l and w, respectively (Fig. S1). The pore size distribution $r(x)$ is characterized as $r(x) = r_i + \lambda x$, where r_i is the pore size at the inlet and λ is the pore size gradient. There is no variation of pore size in the y direction. The pore size at the outlet r_o is dictated by λ defined as $\lambda = r_o - r_i/l$, where $\lambda < 0$ indicates $r_o < r_i$ and $\lambda > 0$ indicates $r_o > r_i$. The number of pores n along the y direction is uniform, and the porosity of the model is given as ω. The invading fluid, of density ρ_1 and viscosity μ_1, displaces the defending fluid, of density ρ_2 and viscosity μ_2, at a constant flow rate Q (Fig. S1). The front advances in the x direction at a constant injection velocity of U and pore velocity of ν. The fluids are immiscible, with interfacial tension given as σ, and the contact angle between interface and grain surface along the defending fluid is denoted as θ. The viscosity ratio of defending fluid and invading fluid is represented by $M = \mu_2/\mu_1$.

Derivation of Stability Criterion Using Linear Stability Analysis

The front is moving in the x direction, and y is transverse direction, as shown in Fig. S1. The governing equations in our case are

Darcy's law

$$\boldsymbol{u}_i = -\frac{k_i}{\mu_i}\nabla(p_i + \rho_i g x) \text{for } i = 1,2 \qquad \textbf{[S1]}$$

and the continuity equation for an incompressible flow

$$\nabla . \boldsymbol{u}_i = 0 \qquad \textbf{[S2]}$$

where $\boldsymbol{u}_i$, k_i (m^2), μ_i, and p_i (pascals) are, respectively, velocity, permeability, viscosity, and average pressure of fluid i. The subscripts 1 and 2 refer to the invading and defending fluid, respectively. Darcy's law can further be written in terms of the flow potential

$$\phi_i = -\frac{k_i}{\mu_i}(p_i + \rho_i g x) \qquad \textbf{[S3]}$$

and substituted into the continuity equation to yield

$$\nabla^2 \phi_i = 0 \qquad \textbf{[S4]}$$

for each fluid flow potential. Saffman and Taylor (10) obtained the solution to Eq. **S4** as

$$\phi_1 = Uh' e^{\alpha t + i\gamma y} + \frac{\alpha h'}{\gamma} e^{\gamma \bar{x}} e^{\alpha t + i\gamma y} \qquad \textbf{[S5]}$$

$$\phi_2 = Uh' e^{\alpha t + i\gamma y} - \frac{\alpha h'}{\gamma} e^{-\gamma \bar{x}} e^{\alpha t + i\gamma y} \qquad \textbf{[S6]}$$

where α is the growth rate, γ is the wavenumber, $h' e^{\alpha t + i\gamma y}$ is the position of perturbed displacement front relative to the base state, and $\bar{x} = x - Ut$. Unlike the traditional case where $p_1 = p_2$, here we state that the pressure difference across the interface (the dynamic boundary condition) is governed by the Young–Laplace equation which introduces the capillary pressure across the interface. Therefore, the resulting equation can be written as

$$\left[Uh' e^{\alpha t + i\gamma y} - \frac{\alpha h'}{\gamma} e^{\alpha t + i\gamma y}\right]\frac{\mu_2}{k_2} - \left[Uh' e^{\alpha t + i\gamma y} + \frac{\alpha h'}{\gamma} e^{\alpha t + i\gamma y}\right]\frac{\mu_1}{k_1} - \Delta\rho g h' e^{\alpha t + i\gamma y} = \frac{2\sigma\cos(\theta)}{r(x)}. \qquad \textbf{[S7]}$$

In contrast to a Hele-Shaw cell, k_i in a porous medium is a function of both pore geometry and the fluid saturation. Therefore, $k_2(x)$ can be computed as $\int dk_2 = -(dr/d\bar{x})\int (dk_2/dr)d\bar{x}$; expressing $\int (dk_2/dr)d\bar{x} = 2r(x)h' e^{\alpha t + i\gamma y}$ and $dr/d\bar{x} = \omega\lambda/n$ results in

$$k_2 = \frac{-2\omega\lambda r(x) h' e^{\alpha t + i\gamma y}}{n} \qquad \textbf{[S8]}$$

where $2\omega\lambda r(x)/n$ and $h' e^{\alpha t + i\gamma y}$ quantify the effects of porous media geometry and the fluid saturation (which varies with position of the front) on k_2, respectively. Furthermore, the stability analysis has been performed around the region where $k_1 = k_2$, which modifies Eq. **S7** as

$$\frac{\alpha}{\gamma U}[M+1] = \frac{\omega 4\sigma\cos(\theta)\lambda}{nU\mu_1} - [1-M] + \frac{2\omega\lambda\Delta\rho r(x) g h' e^{\alpha t}\cos(\gamma y)}{nU\mu_1} \qquad \textbf{[S9]}$$

where M is the viscosity ratio of defending fluid over invading fluid. Note that $\alpha > 0$ corresponds to unstable patterns, and $\alpha < 0$ indicates the stable displacement. Therefore, to determine the stability criterion, one can solve the above relationship for $\alpha = 0$, which will result in critical capillary number Ca_c as

$$Ca_c = \frac{4\lambda\omega\cos(\theta)}{n[1 - M - G]} \qquad \textbf{[S10]}$$

where $G = 2\omega\lambda\Delta\rho r(x) g h'/nU\mu_1$. Combining the Ca_c with the definition of Ca^* given as

$$Ca^* = \frac{Car_i l}{\cos(\theta)\omega\left(4r_i^2 + 6r_i\lambda l + 2\lambda^2 l^2\right)} + \frac{Bol}{2r_i + \lambda l} \qquad \textbf{[S11]}$$

will provide us with stability criterion in the form of critical generalized capillary number Ca_c^* as shown in Eq. **S12**.

$$Ca_c^* = \frac{2\lambda r_i l}{n\left(2r_i^2 + 3r_i\lambda l + \lambda^2 l^2\right)[1 - M - G]} + \frac{Bol}{2r_i + \lambda l}. \qquad \textbf{[S12]}$$

Validation of Stability Criterion at Different Viscosity Ratio, Contact Angle, and Length Scale

The comparison between the analytical equation (Eq. **S12**) under different viscosity ratio M, contact angle θ, and length scale l is shown in Figs. S2–S4, respectively.

Fig. S2 shows that, as M increases, although Ca^* remains constant (this is because the viscosity of invading fluid μ_1 was kept constant), for a given λ, the value of Ca_c^* predicted from Eq. **S12** decreases (decrease in the yellow shaded region and increase in the red shaded region). Furthermore, Fig. S2 demonstrates that, under a constant capillary number Ca, to stabilize the front at higher M values, the pore size gradient has to be

increased. As the contact angle θ increases, the analytically predicted Ca_c^* (Eq. **S12**) remains constant; however, it varies Ca^*. For each λ, the value of Ca^* increases when θ increases. Similar to the case of M, as θ increases, a much sharper gradient in pore size (increase in λ) is required to hinder the growth of viscous fingers. This can be ascribed to decrease in the strength of resistive capillary forces. In addition, we also performed simulations at constant λ conditions but different length scales of l = 0.8, 8.0, and 80 mm.

Pore-Scale Mechanisms Suppressing VF in Ordered Porous Media

Our pore-scale analyses enabled us to determine two invasion mechanisms responsible for suppressing VF, named (*i*) overlap (38, 39) and (*ii*) intermittent burst. Although fundamentally different, these pore-scale displacement mechanisms are nonlocal and exhibit cooperative behavior. During overlap, two neighboring interfaces merge to form a new stable interface (the white dashed line in Fig. S5*A*). The key role of overlap in the formation of a uniform displacement front has been observed in many investigations (14–16). However, neighboring interfaces show the opposite effect during the intermittent burst mechanism (Fig. S3*B*), as one interface recedes (the black dashed line), assisting the adjacent interface to move forward (the white dashed line) (40–43). In comparison with the viscous instability that occurs during VF (where later movement of front is impeded by the dynamic viscocapillary equilibrium), waiting (pinning) time (42) for the interface to drain a pore is significantly longer during intermittent burst as indicated in Fig. 3*F*. It should be noted that the microfingering phenomenon illustrated in *Numerical Simulations* section of the main text is a macroscopic result of the intermittent burst mechanism. Moreover, the frequency of overlap f_O (%) and intermittent burst f_b (%) mechanism has been computed for each simulation case (Fig. S5 *C* and *D*). It can be seen from Fig. S5 *C* and *D* that increasing flow rate weakens the impact of overlap and intermittent burst mechanism on the displacement dynamics, causing instabilities to govern the interfacial displacement and thus resulting in VF. Furthermore, Fig. S5 *C* and *D* demonstrates the change in the dominant pore-scale displacement mechanism from the overlap to intermittent burst mechanism as the magnitude of λ increases.

The identified pore-scale mechanisms control not only the morphology of displacement front but also the evolution of phase pressure difference δp [defined as $p_i - p_o / r_i p_o$, where p_i and p_o correspond to the inlet and outlet pressure (atmospheric pressure), respectively] as illustrated in Fig. S5*E*. Although increasing δp is one of the characteristics of the stable displacement regime (44), how it really increases depends strongly on the processes occurring at the pore scale. Our results show that, when the overlap is the dominant mechanism, δp gradually increases; however, in ordered media where the intermittent burst is the dominant displacement mechanism, δp increases exponentially (Fig. S5*E*).

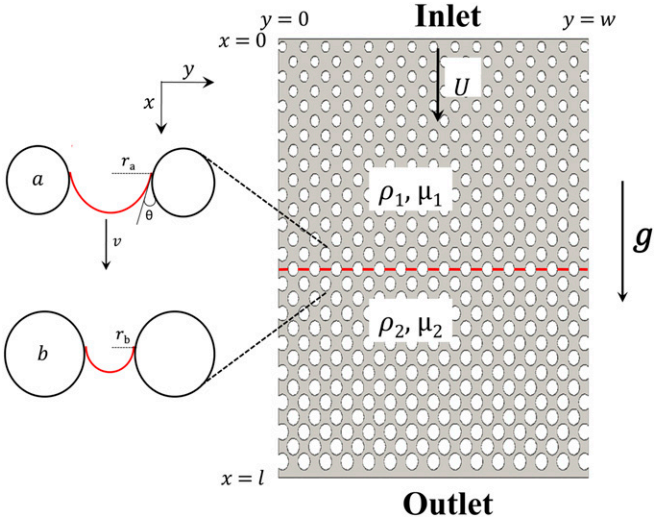

Fig. S1. Schematic of the model used for the analytical analysis. White represents grains, and red shows the interface between two immiscible fluids 1 and 2, where fluid 1 represents the invading fluid and fluid 2 represents the defending fluid.

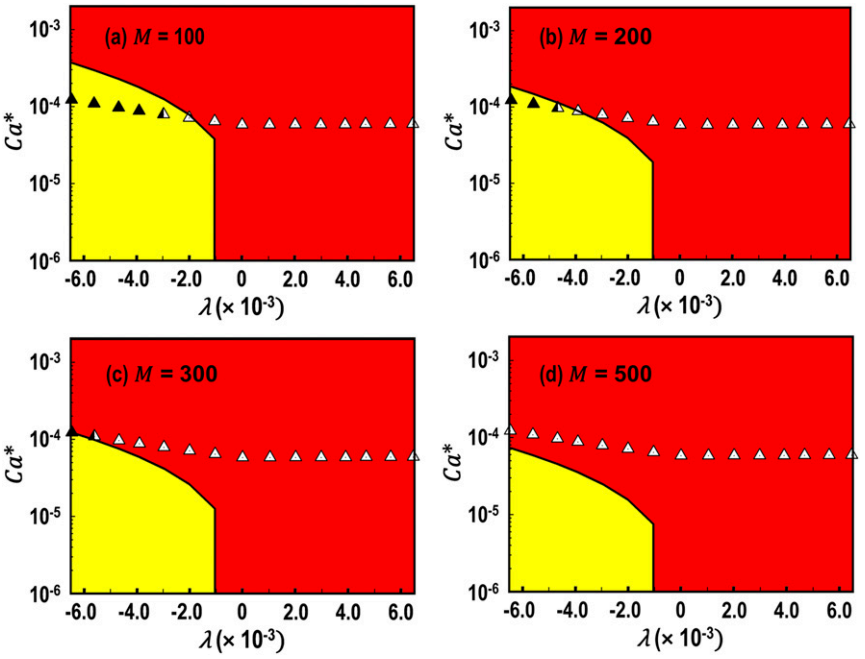

Fig. S2. Relationship between generalized capillary number Ca^* and λ for M equal to (*A*) 100, (*B*) 200, (*C*) 300, and (*D*) 500 at $Ca = 3.2 \times 10^{-6}$. The viscosity of the invading fluid $\mu_1 = 10^{-3}$ Pa·s, while the viscosity of defending fluid μ_2 is allowed to vary. The solid line indicates the analytically predicted Ca_c^*, which is a solution of the stability criterion derived from linear stability analysis (Eq. **S12**). The symbols are the results obtained by the direct numerical simulation where filled, half-filled, and open symbols represent the stable front, Ca_c^*, and unstable front, respectively. Yellow and red regions mark analytically predicted stable and unstable regions separated by the solid line predicted by Eq. **S12**.

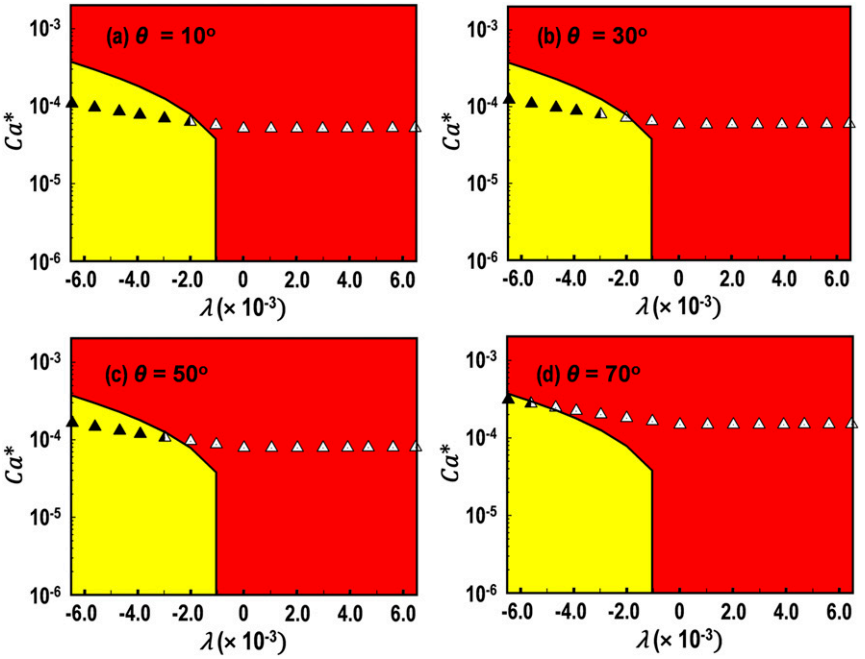

Fig. S3. Relationship between generalized capillary number Ca^* and λ for θ equal to (*A*) 10°, (*B*) 30°, (*C*) 50°, and (*D*) 70° at $Ca = 3.2 \times 10^{-6}$. The viscosity of the invading and defending fluids were constant at 10^{-3} Pa·s and 10^{-1} Pa·s, respectively. The solid line indicates the analytically predicted Ca_c^*, which is a solution of the stability criterion derived from linear stability analysis (Eq. **S12**). The symbols are the results obtained by the direct numerical simulation where filled, half-filled, and open symbols represent the stable front, Ca_c^*, and unstable front, respectively. Yellow and red regions mark analytically predicted stable and unstable regions, respectively, separated by the solid line predicted by Eq. **S12**.

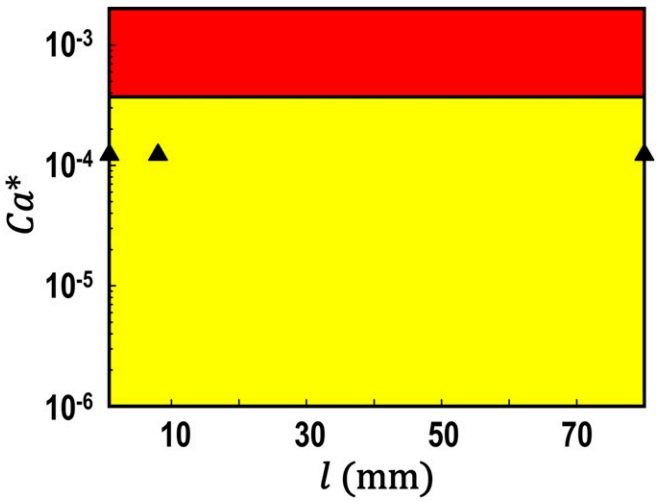

Fig. S4. Relationship between generalized capillary number Ca^* and l with $\lambda = -6.5 \times 10^{-3}$, $\theta = 30°$, $Ca = 3.2 \times 10^{-6}$, and M = 100. The solid line indicates the analytically predicted Ca_c^*, which is a solution of the stability criterion derived from linear stability analysis (Eq. **S12**). The symbols are the results obtained by the direct numerical simulation representing stable front. Yellow and red regions mark analytically predicted stable and unstable regions, respectively, separated by the solid line predicted by Eq. **S12**.

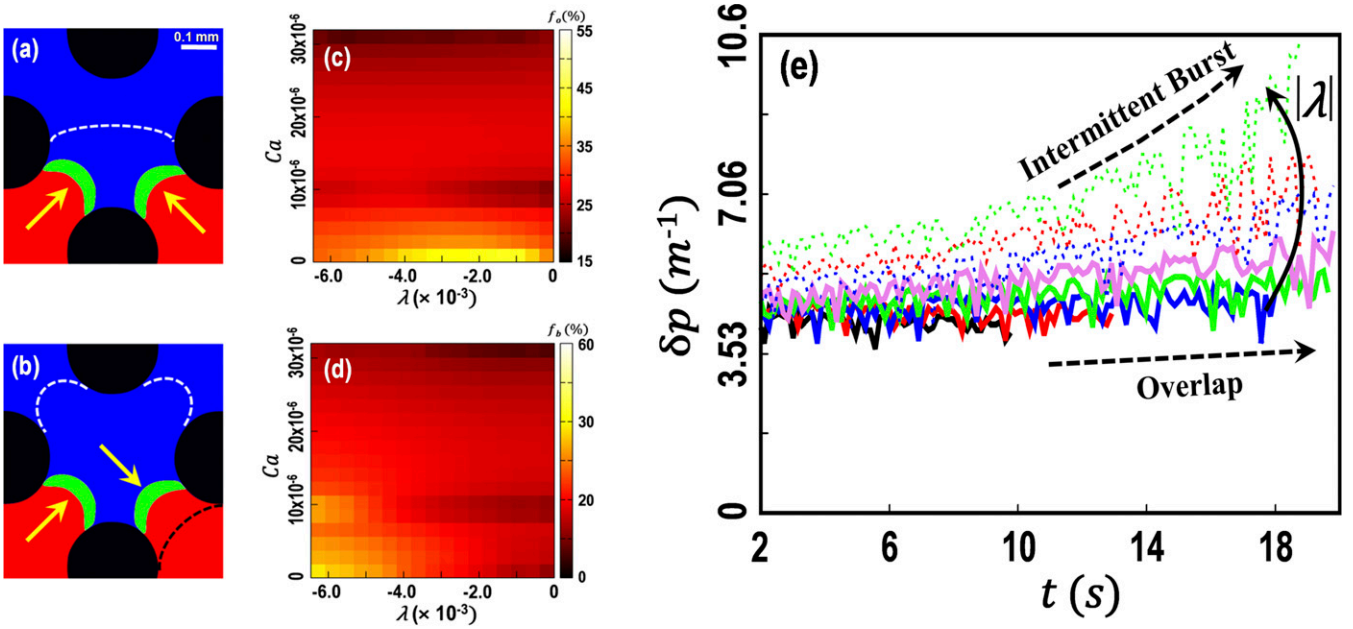

Fig. S5. Pore-scale mechanisms controlling the stability of a front at the macroscopic level. Schematic illustration of the pore-scale (*A*) overlap and (*B*) intermittent burst mechanisms influencing the dynamics of displacement. In *A* and *B*, red, blue, black, and green represent, respectively, invading fluid, defending fluid, grains, and the positions of interfaces before the respective pore-scale displacement mechanism. The direction of displacement is from bottom to top, and movement of each individual interface is shown by the arrows. During the overlap mechanism (*A*), two neighboring interfaces coalesce to form a stable interface (the white dashed line). In the intermittent burst mechanism, one interface advances toward downstream pores (the white dashed line), while the other interface recedes toward the upstream pore (the black dashed line). The 2D color map shown in *C* and *D* indicates the frequency distribution of overlaps f_O (%) and intermittent bursts f_b (%), respectively, versus *Ca* and λ. (*E*) Evolution of the phase pressure difference δp (m^{-1}) defined as $(p_i - p_o)/(10 r_i p_o)$ at $Ca = 3.2 \times 10^{-6}$, where p_i and p_o correspond to the inlet and outlet (open to atmosphere) pressure, respectively. The colors correspond to different values of λ.